


Formation of a Dirac Cone and Dynamic Control of its Half-Metallic Properties Using Double-Layer Ring Dipole Arrays

Go Itami^{✉*} and Osamu Sakai

Department of Electronic Systems Engineering, The University of Shiga Prefecture, 2500 Hassaka-cho, Hikone, Shiga, 522-8533, Japan

 (Received 19 February 2023; revised 23 July 2023; accepted 10 August 2023; published 7 September 2023)

Dirac cone formation and a method for dynamically controlling the band gap using double-layer ring dipole arrays (RDAs) are demonstrated and proposed. The design is mainly based on the composite right-handed–left-handed circuit theorem. It is theoretically and analytically confirmed that the Dirac cone appears at the optimum separation in double-layer RDAs, which are known to have surface-wave modes in the case of a single-layer RDA. It is also found that the band gap can be formed and controlled by decreasing the separation between the two layers. The Dirac cone formation and its dynamic control method on the artificial structure will open the possibility of new transistor applications as an artificial electronic material showing the properties of Dirac half-metals.

DOI: [10.1103/PhysRevApplied.20.034012](https://doi.org/10.1103/PhysRevApplied.20.034012)

I. INTRODUCTION

Topological materials have attracted much attention in recent years, starting with the theoretical proposal of topological insulators [1–9]. The first topological insulating system was proposed even earlier, with the experimental verification of the integer quantum Hall effect in 1980 [1]. A characteristic of topological insulators in a broader definition, which is extended to three-dimensional systems as well as two-dimensional systems where the quantum Hall effect has been observed, is that the bulk of the material exhibits insulating properties, while its surface exhibits a metallic state [2–4,8]. Topological half-metals that exhibit Dirac cones not only on the surface but also in the bulk itself are attracting attention [5–7,9], and one of the typical structures is a Dirac half-metal, which was theoretically proposed in 2012 [9]. The band gap is closed for topological reasons, and the Dirac cone is doubly degenerate with respect to the spin [5,6]. Since the discovery of graphene, Dirac cones have been found to occur in various other natural materials. In particular, methods to control the band gap have attracted much attention because they lead to new transistor possibilities or drastic improvements in transistors [10–13]. For example, typical methods to control the band gap of graphene include the application of an electric field to double layers of graphene and graphene nanoribbons [10,11]. It was confirmed in 2020 that topological properties are manifested not only in electronic systems in solids but also in light within the periodic structure of dielectric materials. Here, bound states in

the continuum (BIC) have been observed as optical topological singularities (when the topological number is an integer) as one of the topological phenomena of light, and the relationship between artificial periodic structure materials and topological materials has become clear [4,14]. The same relationship with BIC modes has been shown in the case of conducting periodic structures [15,16].

The Dirac cone appears not only in electron systems in solids but also in electromagnetic fields in conducting periodic structures [17–22]. It is one of the characteristic phenomena of metasurfaces. The theoretical concept of a Dirac cone metasurface was proposed in 2012 [17,18]. Its existence has been experimentally verified on the basis of the composite right-handed–left-handed (CRLH) circuit theorem [19,20]. Some studies on the applications of a Dirac cone metasurface such as a leaky-wave antenna and an electromagnetic absorber have also been reported [21,22]. As well as Dirac cone in electron systems in solids, Dirac cone metasurfaces also have the potential of application to waveguide and nonlinear devices [23–25]. However, conventional Dirac cone metasurfaces have the problem of forming a band gap from the Dirac cone state, and it is also difficult to control these states successfully, although the properties can be changed by change of the structural parameters.

In this study, analytical and computational results confirm that double layers of ring dipole arrays (RDAs) can produce a Dirac cone property; the double layers of RDAs seem to be simple but include sufficient geometrical parameters for achieving dispersion relations similar to those achieved with Dirac half-metals. By changing of the separation between the layers, the Dirac cone state can be changed to a band-gap-forming state and the band can

*ot68gitami@ec.usp.ac.jp

be controlled. As a three-dimensional photonic topological insulator shows quadratic dispersion of topological surface states based on spoof surface plasmon polaritons (SSPPs), the proposed band-control technique is partially consistent with this study [8]. An RDA is a perforated structure of metal-plate arrays that is known as an SSPP structure [26]. It is also known that RDAs with a single layer generate surface waves (SSPPs) or convert to BIC mode, and the Dirac cone state does not appear until double layers are stacked [16]. A Dirac cone metasurface with a dynamically controllable band gap could lead to the realization of artificial electronic materials without the restrictions that natural materials such as graphene are subject to due to their physical properties. For example, when one is controlling the band of the Dirac cone with graphene, the operational risk is high because of the configuration that maintains the OFF state in the voltage-applied state when a voltage is applied, and advanced molecular-design techniques are required for nanoribbons, so reproduction of electronic properties in graphene by artificial materials will fundamentally expand the range of applications as transistors [10,27,28]. From the viewpoint of physical properties, graphene is characterized by both plasmon modes based on material properties and Dirac cones based on topological properties. In the metasurface, the key factor connecting

the plasmonics and the Dirac cone is the interference effect of the surface waves produced by the two-layer structure of the RDAs using the BIC mode. The two factors can be made compatible by use of a toroidal-dipole model, which was originally for the plasmonic nanoparticle chain that shows BIC modes while being protected by symmetry [16,29]. If metasurfaces can replace graphene as an artificial electronic material, this will lead to a breakthrough in optoelectronic fusion devices used in integrated circuits that support such as artificial intelligence, because it will broaden the range of device designs based on the interaction between light and electrons and make them easier to manufacture [30].

II. THEORY AND OPERATION PRINCIPLE

The RDA shown in Fig. 1(a) has a spatial configuration with $d = 3$ mm, $a = 2$ mm, $p = 1.6$ mm, and $w = 3$ mm. In the case of a single-layer RDA, the structure exhibits a conversion state from a spoof-surface-plasmon mode to a BIC mode when the inner ring size (p) is changed [16]. The BIC mode is usually not manifested in a symmetry-protected state, but is manifested in a symmetry mode following a plasmonic nanoparticle chain [29]. This structure is based on the toroidal-dipole model, which follows

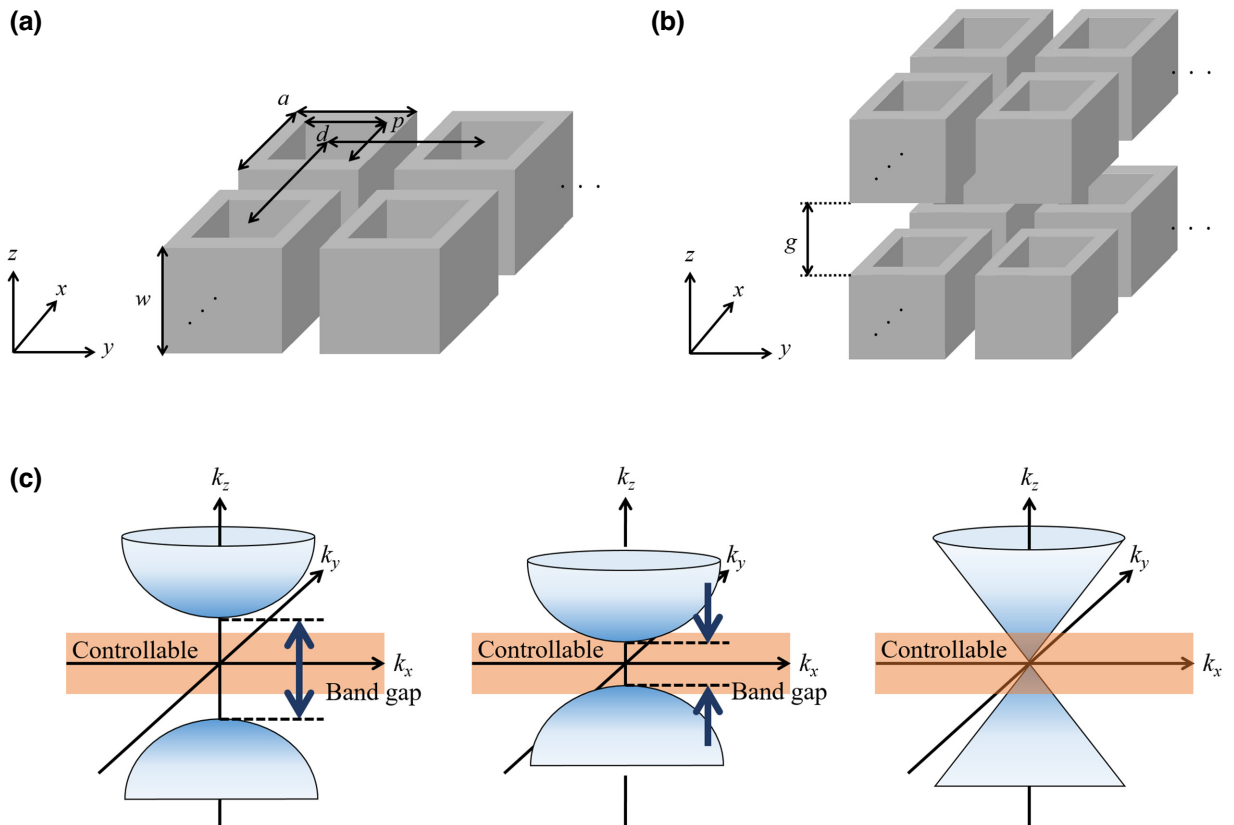


FIG. 1. (a) A single-layer ring dipole array. (b) A double-layer ring dipole array. (c) Change of the band gap with change of separation g .

the symmetric mode according to the plasmonic nanoparticle chain, and is a symmetry-protected BIC structure. The Dirac cone state does not appear as it is. However, as shown in Fig. 1(b), when two RDA layers are stacked, interactions between the structures are created, and at a certain separation g , a Dirac cone is produced. When the separation is reduced, the band shifts and a band gap is formed as shown in Fig. 1(c). In other words, by changing of the separation (g) of the RDAs, the Dirac cone state can be formed and the band can be controlled. These changes in band structure can be explained by use of the wave theory involved in SSPP generation and the circuit theory involved in CRLH transmission lines. The relationship between the propagation state, separation g , and band structure is explained separately for a single-layer RDA and a double-layer RDA. First, in the case of a single-layer RDA, only surface-wave modes with the dispersion relation of SSPPs are generated, and they can be regarded as behaving like a metal propagating on the surface of the structure. Therefore, one surface-wave mode appears as

the fundamental mode. The following explains the operating principle, with use of Fig. 2. First, the dispersion relation of surface modes in the case of a single-layer RDA is as follows [16,26]:

$$\omega^2 = \frac{c^2 k_{\parallel}^2}{1 - \mu_m / \epsilon_m}, \quad \epsilon_m = \frac{1}{\mu_m} \left(1 - \frac{\omega_p^2}{\omega^2} \right), \quad (1)$$

where c is the speed of light, ω is the angular frequency, k_{\parallel} is the wave number of the surface mode, and ω_p , ϵ_m , and μ_m are the cutoff angular frequency, the effective permittivity, and the effective magnetic permeability of the RDA, respectively. In the single-layer case, ω and k_{\parallel} are determined according to Eq. (1). ω_p and μ_m are uniquely determined by only the structural parameters. ϵ_m depends only on ω as a variable, and the dispersion relation is uniquely determined by the structural parameters [16,26].

The case of a double-layer RDA differs from the case of a single-layer RDA in that it exhibits a two-band structure. The reason for this can be explained by circuit

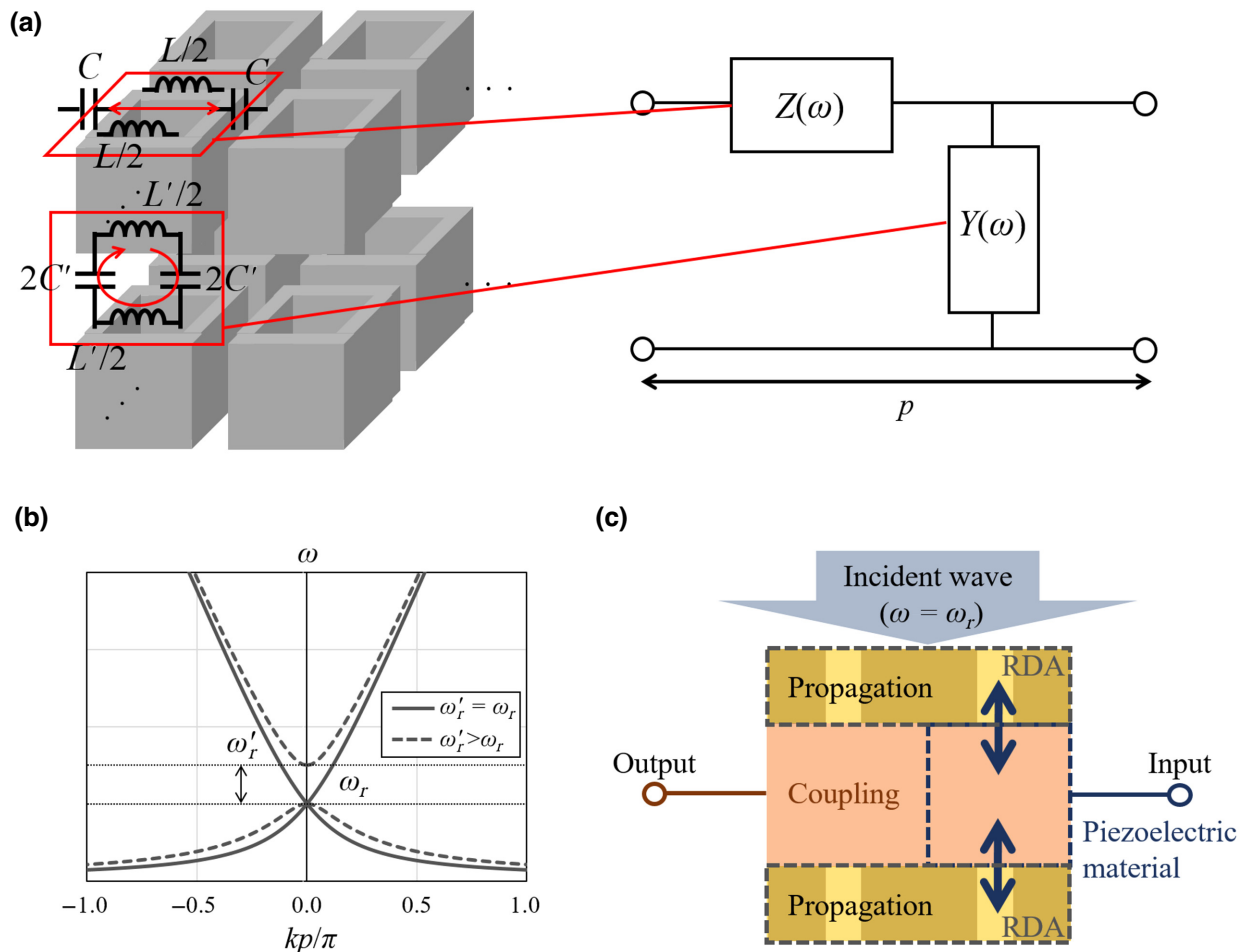


FIG. 2. (a) Equivalent-circuit model for the double-layer ring dipole array. (b) Dispersion relation of the equivalent-circuit model. (c) Modulation or amplification mechanism of the double-layer ring dipole array.

theory. Since the modes of propagation interact between the layers, a double-layer RDA can be described as a CRLH-transmission-line model, as shown in Fig. 2(a). First, the upper or lower layer acts as a series resonator because inductors and capacitors are formed between the ring dipole and adjacent structures, respectively. Between the upper and lower layers, the capacitors formed between adjacent ring dipoles and the inductors possessed by the ring dipoles act as parallel resonators. If the series-resonance and parallel-resonance actions are represented by $Z(\omega)$ and $Y(\omega)$, respectively, the dispersion relation in the infinite periodic array of the unit structure including these circuits can be expressed as follows, where propagation within the structure is assumed to be lossless:

$$\begin{aligned} \cosh(ikp) &= 1 + Z(\omega)Y(\omega), \\ Z(\omega) &= i \left(\omega L - \frac{1}{\omega C} \right), \\ Y(\omega) &= i \left(\omega C' - \frac{1}{\omega L'} \right), \end{aligned} \quad (2)$$

where L and C are the inductors and capacitors contributing to the series resonance, respectively, and L' and C' represent the inductors and capacitors that contribute to the parallel resonance, respectively. From Eq. (2), the angular frequency ω at the Γ point ($k = 0$) is derived as $\omega = 1/\sqrt{LC}, 1/\sqrt{L'C'}$. Since $C \geq C'$ from the structure, $\omega_r' \geq \omega_r$ ($\omega_r = 1/\sqrt{LC}, \omega_r' = 1/\sqrt{L'C'}$).

Figure 2(b) shows the dispersion relation of Eq. (2). A Dirac cone is formed when $\omega_r' = \omega_r$. The inductance L and capacitance C depend only on the structure of the RDA and are not affected by changes in the separation g . On the other hand, for L' and C' , the influence of the separation g should be carefully considered. In a general transmission line, C' is expected to vary with the separation g according to the circuit theory. However, C' is almost unaffected because the surface-wave mode does not propagate in the z direction. Conversely, the current flowing in the inductance L' is considered to be affected by the separation g because it flows in the direction in which the surface wave propagates. Assuming that the inductance model follows the parallel-line inductance model, the inductance can be expressed as $L' = L'_0 \ln 2[1 + (g/w)]$ [31]. Here, since the inductances L and L' and the capacitances C and C' are functions of the structural parameters of the double-layer RDA, they can be expressed as $L = L(a, p, w)$, $C = C(d, a, p, w)$, $L' = L'_0(a, p, w) \ln 2[1 + (g/w)]$, and $C' = C'(d, a, p, w)$. The separation g at the Dirac point is obtained by solving $\omega_r = \omega_r' \Leftrightarrow 1/\sqrt{L(a, p, w)C(d, a, p, w)} = 1/\sqrt{L'_0(a, p, w) \ln 2[1 + (g/w)]C'(d, a, p, w)}$. The separation g at the Dirac point can be derived in the following

form:

$$g_D = w \left[\frac{1}{2} \exp \frac{L(a, p, w)C(d, a, p, w)}{L'_0(a, p, w)C'(d, a, p, w)} - 1 \right]. \quad (3)$$

From the above discussion, as the separation g becomes smaller, ω_r' becomes larger and the band gap becomes larger. Similarly, as the separation g increases, ω_r' decreases and the band gap decreases. When $\omega_r' = \omega_r (= \omega_D)$, zero band gap is reached and a state similar to the Dirac cone appears. This is discussed later. The band gap that appears in the double-layer RDA depends mechanically on the separation g and electromagnetically on the circuit model. In other words, by the setting up of a mechanism that converts electrical response to mechanical response, such as a piezoelectric element between the layers, the circuit constant (inductance L') can be changed and the band gap can be controlled. When a band gap exists in the double-layer RDA ($\omega_r' > \omega_r$), it represents a mixture of propagating modes (ω_r) on the surface of the single-layer RDA and coupled modes (ω_r') formed by the interaction between the layers. Therefore, when a wave of ω_r is incident, only the surface-wave mode propagating on the RDA (ω_r) is excited, and the coupled modes between the layers are not excited. For example, as shown in Fig. 2(c), a piezoelectric element is placed between the layers and the separation g changes according to the input electrical signal, and the band gap changes accordingly to zero. In the zero-band-gap state, the propagation mode and the coupling mode coincide ($\omega_r' = \omega_r$), and the coupling mode between the layers is simultaneously excited by the incident wave of ω_r . In other words, the band gap can be described as the input energy required to create a coupled mode between layers. With a wave of ω_r continuously incident on the double-layer RDA with piezoelectric elements installed between the layers as described above, the signal sent to the piezoelectric elements as input and the signal obtained from the coupled-mode transmission line between the layers as output is considered to have a modulation or amplification effect. The controllability of the band gap focusing on the inductance is discussed here; however, similar control by application of an electric field focusing on the capacitance is also expected to be possible by change of the structure correspondingly. From the discussions, it is possible to control the propagation state in which the band gap is changed by an externally applied input signal, and surface-wave modes of the frequency that the single-layer RDA can originally have propagate while coupling between the layers. Therefore, the modulation function of surface-wave modes can be realized without the use of semiconductors. In other words, in terms of material properties, if the band gap exceeds the range that can be controlled by the separation g , the material is effectively regarded as an insulator,

and if it falls within the range, it is regarded as a semiconductor. Finally, zero-band-gap states are discussed in more detail. More precisely, each surface-wave mode in the two layers is subject to multiwave interference; therefore, an ideal Dirac cone is not formed and a zero-band-gap state with some nonlinearity is created. However, assuming that this mechanism is similar to the mechanism in semiconductors as discussed above, it will be possible to achieve high-speed operation due to the behavior of electrons so that they obey the theory of relativity. In the following, the interference between two layers of surface-wave modes is discussed on the basis of wave theory to consider the zero-band-gap states.

In the two-layer case, as shown in Fig. 3(a), it is generally necessary to solve a multiwave interference problem rigorously with boundary conditions of three regions, which is complicated and difficult to achieve in practice. However, if the separation g is less than or almost equal to the wavelength, there is little interference due to propagation, and regions I–III can be regarded as a single effective medium as region I' [32]. In this case, the Dirac point is considered by replacement of the effective dielectric constant and effective magnetic permeability in Eq. (1) with ϵ'_m and μ'_m , and solving $k_{\parallel} = 0$ under the condition $\omega > 0$. Here, when one is considering the interference effects between layers, note that when k_{\parallel} is near 0, the interference effects become large due to the near-perpendicular incidence condition, and the medium can no longer be regarded as a single effective medium, and therefore ω_D can be an approximate value. In the dispersion relation of the RDA obtained from Eq. (1), $\partial k_{\parallel} / \partial \omega \rightarrow \infty$ ($\partial \omega / \partial k_{\parallel} \rightarrow 0$) for $k_{\parallel} \rightarrow 0$. However, for the reasons described above, this model changes and $\partial k_{\parallel} / \partial \omega$ converges to a finite value ($1/v_D$), resulting in a nearly linear dispersion relation. Therefore, the Dirac equation can be described as below, and linear dispersion near the point of

$\omega = \omega_D$ is obtained [33]:

$$H \begin{bmatrix} \psi_1 \\ \psi_2 \end{bmatrix} = \delta\omega \begin{bmatrix} \psi_1 \\ \psi_2 \end{bmatrix},$$

$$H = \begin{bmatrix} 0 & -iv_D(\partial_x - i\partial_y) \\ -iv_D(\partial_x + i\partial_y) & 0 \end{bmatrix},$$

$$\delta\omega = \omega - \omega_D. \quad (4)$$

Therefore, $\delta\omega^2 = v_D^2(k_x^2 + k_y^2) = k_{\parallel}(\omega)^2 \Leftrightarrow \delta\omega = \pm v_D k_{\parallel}(\omega)$, and from Eq. (1), we have

$$k_{\parallel}(\omega) = \left(\frac{\omega}{c}\right) \sqrt{1 + \frac{\omega^2 \mu_m'^2}{\omega_p^2 - \omega^2}} (=F(\omega)). \quad (5)$$

Finally, the dispersion relation around $\omega = \omega_D$ is expressed as below by application of the Taylor expansion to Eq. (5):

$$k_{\parallel}(\omega)|_{\omega \simeq \omega_D} \simeq F(\omega_D) + F'(\omega_D)(\omega - \omega_D) \simeq \frac{1}{v_D}(\omega - \omega_D). \quad (6)$$

Note that the third and subsequent terms are negligibly small and are omitted [34]. Next, the operating principle of creating the band gap is derived as follows. As shown in Fig. 3(b), in the case of two layers, ω_p changes with the separation g between the layers, so ϵ_m also changes and the dispersion relation is modified. ω_p in the single-layer case is different from ω_p in the two-layer case, and it can be confirmed that ω_p can be controlled by the separation g in the two-layer case. Therefore, the two-layer case can be expressed as $\omega_p(g) \simeq \omega_{p0}f(g)$. Here ω_{p0} is the cutoff angular frequency in the single-layer case and $f(g)$ is the fitting curve shown in Fig. 3(b). Therefore, k_{\parallel}

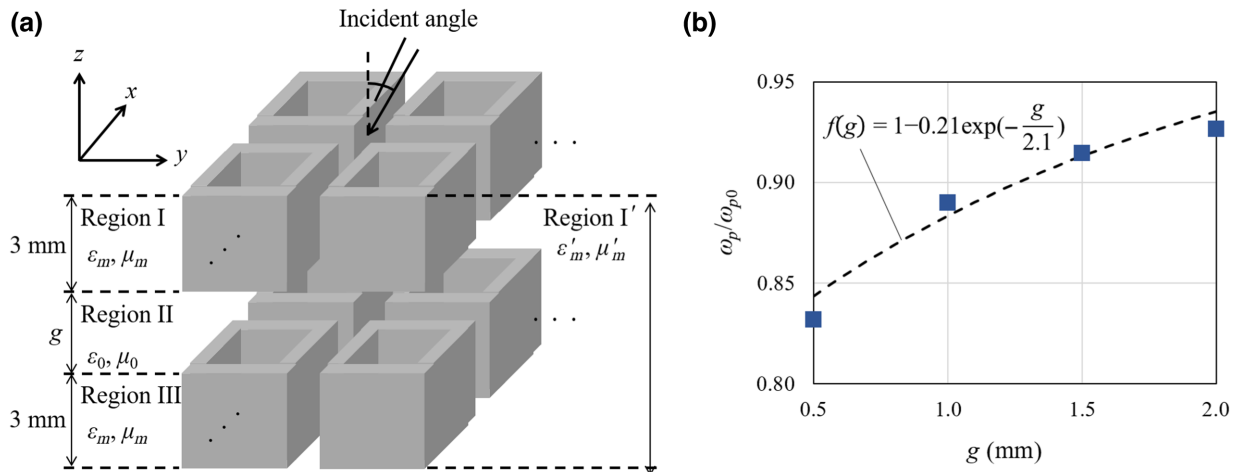


FIG. 3. (a) Propagation model in a double-layer ring dipole array. (b) Dependence of the cutoff angular frequency on g for the parameter set of $d = 3$ mm, $a = 2$ mm, $p = 1.6$ mm, and $w = 3$ mm.

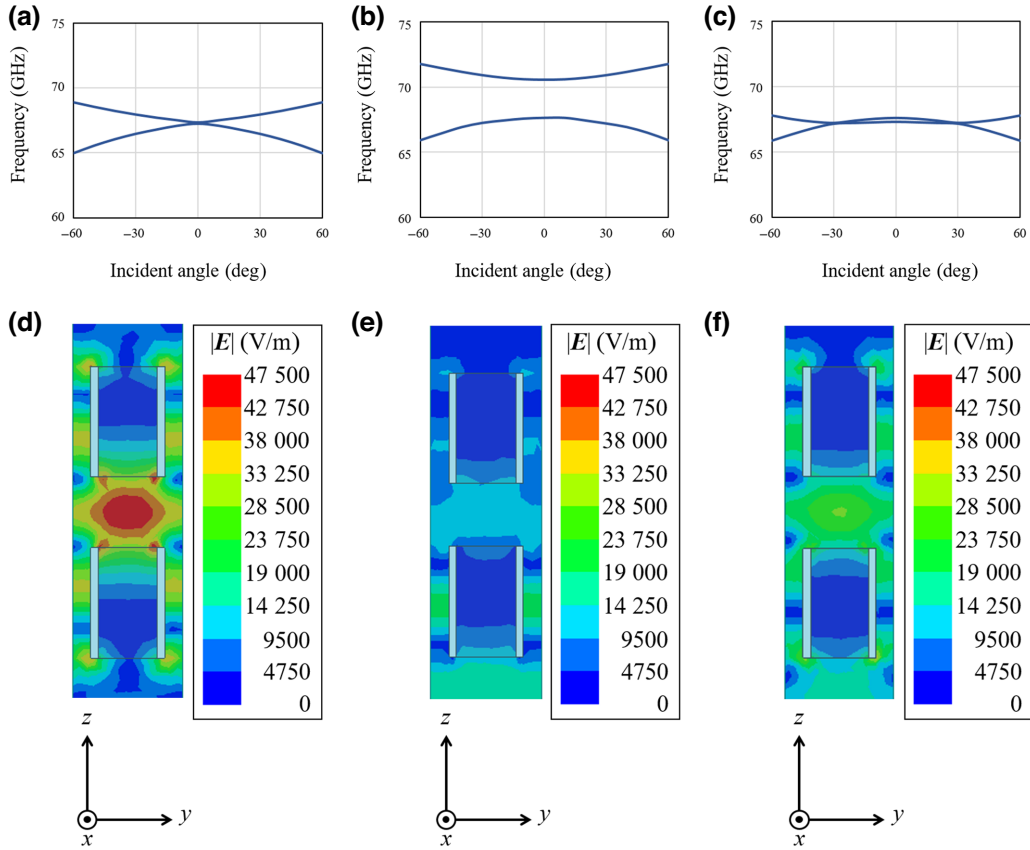


FIG. 4. Results of eigenmode analysis in the case of (a) $g = 1.91$ mm, (b) $g = 1.7$ mm, and (c) $g = 2.0$ mm, and electric field distributions in the case of (d) $g = 1.91$ mm, (e) $g = 1.7$ mm, and (f) $g = 2.0$ mm at 67.6 GHz (which is the Γ point in the Dirac cone state).

can be expressed as $k_{\parallel}(\omega, g) = F(\omega, g)$. Then, as well as in Eq. (6), considering the Taylor expansion of k_{\parallel} for $g \simeq g_D$ at $\omega = \omega_D$, we obtain

$$k_{\parallel}(\omega_D, g)|_{g \simeq g_D} \simeq F(\omega_D, g_D) + \frac{\partial F(\omega_D, g)}{\partial g}|_{g=g_D}(g - g_D) \simeq F'(\omega_D, g_D)(g - g_D). \quad (7)$$

The first term in Eq. (7) can be approximated to 0 as well as the first term in Eq. (6), and considering the value of $f(g_D)$, $F'(\omega_D, g_D)$ converges to a finite value. The third and subsequent terms are negligibly small and are omitted. The above discussion shows that k_{\parallel} can be controlled by g . Therefore, $\delta\omega$ varies with g to create and control the band gap.

III. RESULTS AND DISCUSSION

The dispersion relation in the double-layer RDA was calculated by eigenvalue analysis, and the results are shown in Figs. 4(a)–4(c) for $g = 1.91$ mm, $g = 1.7$ mm, and $g = 2.0$ mm, respectively. From Fig. 4(a), it is

confirmed that the Dirac cone is present for $g = 1.91$ mm. As discussed above, it can be seen that a nearly linear dispersion relation is obtained around $\omega = \omega_D$. On the other hand, Fig. 4(b) shows that a band gap is formed. The band gap is about 4.4% larger than the frequency of the Γ point at the time of Dirac cone formation ($g = 1.91$ mm) in Fig. 4(a). Figure 4(c) shows intersecting bands since the separation g at the Dirac point. The electric field distributions of the double-layer RDA at the frequency (67.6 GHz) of the Γ point during the formation of the Dirac cone are shown in Figs. 4(d)–4(f). These results show the electric field distributions for $g = 1.91$ mm, $g = 1.7$ mm, and $g = 2.0$ mm, respectively. Figure 4(d) shows that the electric field is concentrated at the edges of the ring and between the layers. This is consistent with the proposed theory of surface-wave propagation, which suggests that in the region where the wave number k_{\parallel} approaches 0, the interaction between the layers becomes stronger and the electric field concentrates. On the other hand, Fig. 4(e) shows that the electric field distribution at the edge of the ring and between the layers is weaker than in the case in Fig. 4(d). This shows that the interaction between the layers is weaker than in the case in Fig. 4(d). From

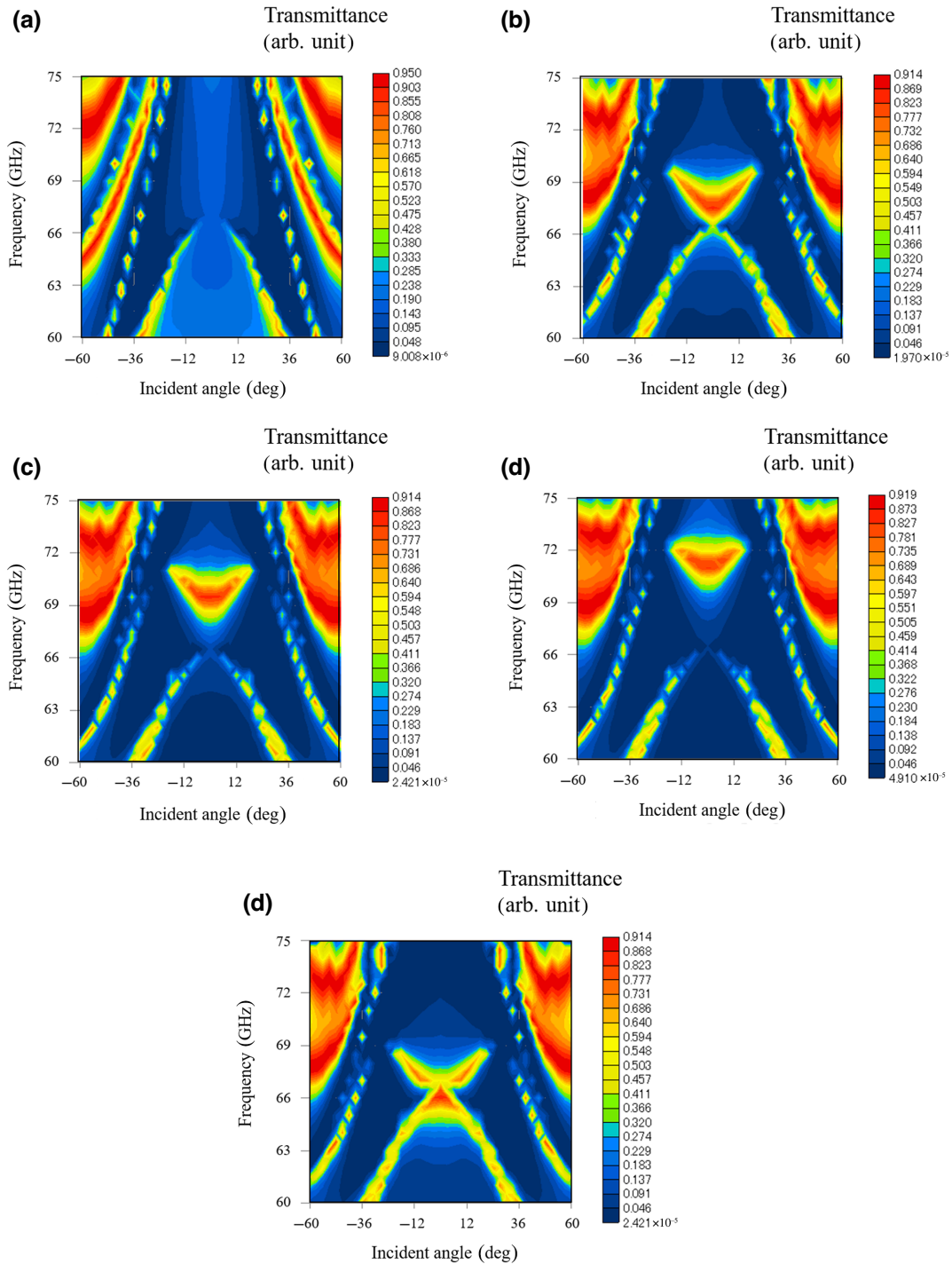


FIG. 5. Results of full-wave analysis in the case of (a) a single-layer ring dipole array and a double-layer ring dipole array with (b) $g = 1.91$ mm, (c) $g = 1.8$ mm, (d) $g = 1.7$ mm, and (e) $g = 2.0$ mm.

comparison of Figs. 4(d) and 4(e), the difference between the presence and the absence of coupled modes is confirmed as the strength of the electric field distribution, which is consistent with the circuit model. It also suggests the feasibility of modulation and amplification functions. In Fig. 4(f) the distribution is weaker than in Fig. 4(d) since the bands intersect around the frequency band. The state is

considered to be the cross modes between the propagation and coupling modes.

Next, the angular dependencies of the transmitted waves in the single-layer RDA and the double-layer RDA were confirmed by full-wave analyses. Figures 5(a)–5(e) show the results for a single-layer RDA and a double-layer RDA with $g = 1.91$ mm, $g = 1.8$ mm, $g = 1.7$ mm,

and $g = 2.0$ mm, respectively. Figure 5(a) shows that lower-frequency bands can be seen in the single-layer RDA, but the higher-frequency band does not exist. This result is also consistent with the circuit-theory approach used to derive the dispersion relation. In other words, since there is no parallel-resonance function based on the concentration of electric fields between the layers, the CRLH circuit structure is not formed, and only a left-handed band with only a series-resonance function remains [19,20]. The results in Figs. 5(b) and 5(d) show that the change in the behavior of the dispersion relation is consistent with the eigenvalue analysis in Figs. 4(a) and 4(b). Namely, Fig. 5(b) shows that the full-wave analysis also confirms the presence of a Dirac cone for $g = 1.91$ mm. Similarly, in Fig. 5(d), it confirms that the band gap opens when g is decreased from 1.91 to 1.7 mm, and the Dirac cone state is transformed. Figures 5(c) and 5(d) show that the band-gap width increases when g is decreased from 1.8 to 1.7 mm. Figures 5(b) and 5(e) show that the bands cross each other when they are closer than in the Dirac cone state. From the above discussion, it is confirmed that the double-layer RDA forms a Dirac cone at the optimum separation and that the band gap can be created and dynamically controlled by variation of the separation g , on the basis of different analysis approaches.

IV. CONCLUSION

Dirac cone formation on double-layer RDAs and a method for dynamic control of the band gap are demonstrated and proposed. The structure is considered to have dispersion relations based on the CRLH-transmission-line theory. It is confirmed that by optimization of the separation between the layers, the Dirac cone is formed, and by decrease of the separation, the Γ points of each band are separated and the band gap is formed and controlled, in eigenvalue and full-wave analyses. This method suggests the possibility of artificial electronic materials with a Dirac cone, and indicates the possibility of new transistor applications.

ACKNOWLEDGMENTS

This work was supported by a Grant-in-Aid for Scientific Research from the Japanese Ministry of Education, Culture, Sports, Science and Technology (JSPS KAKENHI Grants No. JP18H03690 and No. JP22K18704).

-
- [1] K. v. Klitzing, G. Dorda, and M. Pepper, New Method for High-Accuracy Determination of the Fine-Structure Constant Based on Quantized Hall Resistance, *Phys. Rev. Lett.* **45**, 494 (1980).
 [2] B. A. Bernevig and S.-C. Zhang, Quantum Spin Hall Effect, *Phys. Rev. Lett.* **96**, 106802 (2006).

- [3] M. Z. Hasan and C. L. Kane, *Colloquium: Topological insulators*, *Rev. Mod. Phys.* **82**, 3045 (2010).
 [4] T. Yoda and M. Notomi, Generation and Annihilation of Topologically Protected Bound States in the Continuum and Circularly Polarized States by Symmetry Breaking, *Phys. Rev. Lett.* **125**, 053902 (2020).
 [5] Z. Wang, Y. Sun, X. Q. Chen, C. Franchini, G. Xu, H. Weng, X. Dai, and Z. Fang, Dirac semimetal and topological phase transitions in $A_3\text{Bi}$ ($A = \text{Na, K, Rb}$), *Phys. Rev. B* **85**, 195320 (2012).
 [6] Z. Wang, H. Weng, Q. Wu, X. Dai, and Z. Fang, Three-dimensional Dirac semimetal and quantum transport in Cd_3As_2 , *Phys. Rev. B* **88**, 125427 (2013).
 [7] T. Chen, T. Tomita, S. Minami, M. Fu, T. Koretsune, M. Kitatani, I. Muhammad, D. Nishio-Hamane, R. Ishii, F. Ishii, R. Arita, and S. Nakatsuji, Anomalous transport due to Weyl fermions in the chiral antiferromagnets Mn_3X , $X = \text{Sn, Ge}$, *Nat. Commun.* **12**, 572 (2021).
 [8] M. Kim, Z. Wang, Y. Yang, H. T. Teo, J. Rho, and B. Zhang, Three-dimensional photonic topological insulator without spin-orbit coupling, *Nat. Commun.* **13**, 3499 (2022).
 [9] H. Ishizuka and Y. Motome, Dirac Half-Metal in a Triangular Ferrimagnet, *Phys. Rev. Lett.* **109**, 237207 (2012).
 [10] Y. Zhang, T. T. Tang, C. Girit, Z. Hao, M. C. Martin, A. Zettl, M. F. Crommie, Y. R. Shen, and F. Wang, Direct observation of a widely tunable bandgap in bilayer graphene, *Nature* **459**, 820 (2009).
 [11] Y. W. Son, M. L. Cohen, and S. G. Louie, Energy Gaps in Graphene Nanoribbons, *Phys. Rev. Lett.* **98**, 089901 (2007).
 [12] H. Takenaka, S. Sandhoefner, A. A. Kovalev, and E. Y. Tsymal, Magnetoelectric control of topological phases in graphene, *Phys. Rev. B* **100**, 125156 (2019).
 [13] Y. Gao, X. Lin, T. Smart, P. Ci, K. Watanabe, T. Taniguchi, R. Jeanloz, J. Ni, and J. Wu, Band Engineering of Large-Twist-Angle Graphene/ h -BN Moiré Superlattices with Pressure, *Phys. Rev. Lett.* **125**, 226403 (2020).
 [14] Y.-G. Sang, J.-Y. Lu, Y.-H. Ouyang, H.-Y. Luan, J.-H. Wu, J.-Y. Li, and R.-M. Ma, Topological polarization singular lasing with highly efficient radiation channel, *Nat. Commun.* **13**, 6485 (2022).
 [15] S. Sun, Y. Ding, H. Li, P. Hu, C. W. Cheng, Y. Sang, F. Cao, Y. Hu, A. Alù, D. Liu, Z. Wang, S. Gwo, D. Han, and J. Shi, Tunable plasmonic bound states in the continuum in the visible range, *Phys. Rev. B* **103**, 045416 (2021).
 [16] G. Itami and O. Sakai, Independent control method for plasmonic skin depth based on transformation from spoof surface plasmon polaritons to bound states in the continuum, *Phys. Rev. B* **106**, 245406 (2022).
 [17] K. Sakoda, Dirac cone in two- and three-dimensional metamaterials, *Opt. Express* **20**, 3898 (2012).
 [18] K. Sakoda, Double Dirac cones in triangular-lattice metamaterials, *Opt. Express* **20**, 9925 (2012).
 [19] S. Nagai and A. Sanada, Γ -point group velocity of lossy Dirac cone composite right/left-handed metamaterials, *IEICE Electron. Express* **13**, 20160281 (2016).
 [20] A. Sanada, C. Caloz, and T. Itoh, Characteristics of the composite right/left-handed transmission lines, *IEEE Microw. Wirel. Compon. Lett.* **14**, 68 (2004).
 [21] A. Sanada, S. Nagai, and T. Yamamoto, Angle selective high absorption by a mushroom metasurface at

- V-band, Proc. of 2013 Asia-Paific Microwave Conf., T2F-3 (2011).
- [22] A. Sanada and S. Nagai, Extremely high absorption by Dirac cone mushroom metasurfaces in millimeter-wave regions, Proc. 5th Int. Conf. on Metamaterials, Photonic Crystals and Plasmonics, A415 (2014).
- [23] Y. Li, C. T. Chan, and E. Mazur, Dirac-like cone-based electromagnetic zero-index metamaterials, *Light Sci. Appl.* **10**, 203 (2021).
- [24] M. W. Ashraf and M. Faryad, On the mapping of Dirac-like cone dispersion in dielectric photonic crystals to an effective zero-index medium, *J. Opt. Soc. Am. B* **33**, 1008 (2016).
- [25] D. I. Vulis, Y. Li, O. Reshef, P. C. Muñoz, M. Yin, S. Kita, M. Lončar, and E. Mazur, Monolithic CMOS-compatible zero-index metamaterials, *Opt. Express* **25**, 12381 (2017).
- [26] G. Itami and O. Sakai, Analysis and observation of the breakdown of Babinet's principle in complementary spoof surface plasmon polariton structures, *Sci. Rep.* **10**, 11027 (2020).
- [27] Y-M. Lin, C. Dimitrakopoulous, K. A. Jenkins, D. B. Farmer, H-Y. Chiu, A. Grill, and P. H. Avouris, 100-GHz transistors from wafer-scale epitaxial graphene, *Science* **327**, 5966 (2010).
- [28] K. Nishiguchi, H. Yamaguchi, and Akira Fujiwara, Subgahertz Multilayer-Graphene Nanoelectromechanical System Integrated with a Nanometer-Scale Silicon Transistor Driven by Reflectometry, *Phys. Rev. Appl.* **19**, L011003 (2023).
- [29] M. Gong, P. Hu, Q. Song, H. Xiang, and D. Han, Bound states in the continuum from a symmetric mode with a dominant toroidal dipole resonance, *Phys. Rev. A* **105**, 033504 (2022).
- [30] Y. Li, N. An, Z. Lu, Y. Wang, B. Chang, T Tan, X. Guo, X. Xu, J. He, H. Xia, Z. Wu, Y. Su, Y. Liu, Y. Rao, G. Soavi, and B. Yao, Nonlinear co-generation of graphene plasmons for optoelectronic logic operations, *Nat. Commun.* **13**, 3138 (2022).
- [31] F. W. Grover, *Inductance Calculations: Working Formulas and Tables* (Dover, New York, 1946).
- [32] D. W. Mikhail, A. Kats, and F. Capasso, Spoof surface plasmon waveguide forces, *Opt. Lett.* **39**, 517 (2014).
- [33] X. Zhang, Observing *Zitterbewegung* for Photons near the Dirac Point of a Two-Dimensional Photonic Crystal, *Phys. Rev. Lett.* **100**, 113903 (2008).
- [34] J. Zhang, S. Deng, Z. Liu, and Z. Liu, The rare two-dimensional materials with Dirac cones, *Natl. Sci. Rev.* **2**, 22 (2015).